ISBN: 978-953-307-242-5
In book: Coherence and Ultrashort Pulse Laser Emission
Source: InTech
(2010)

25

Two-Photon Polymerization of Inorganic-Organic Hybrid Polymers as Scalable Technology Using Ultra-Short Laser Pulses

Houbertz, Ruth[1], Steenhusen, Sönke[1],
Stichel, Thomas[1,3], and Sextl, Gerhard[1,2]
[1]Fraunhofer ISC, Neunerplatz 2, 97082 Würzburg,
[2]Chemische Technologie der Materialsynthese, Julius-Maximilians-Universität, Röntgenring 11, 97070 Würzburg,
[3]Nano-Optics & Biophotonics Group, Physikalisches Institut, Lehrstuhl für Experimentelle Physik V, Julius-Maximilians-Universität, Am Hubland, 97074 Würzburg, Germany

1. Introduction

For more than five decades, laser light properties have been taken advantage of, mostly using first order interactions between photons and materials. Well-established methods such as laser welding (Sieben & Brunnecker, 2009; El-Bataghy, 1997; Song et al., 2009), laser ablation (Conforti et al., 2007; Baudach et al., 2000; Spyridaki et al., 2003; Blanchet et al., 1993), and direct laser writing (Schweizer et al., 2008; Koechlin et al., 2009) were improved concomitantly with the laser quality (e.g. beam profile) or the laser energy (e.g. short laser pulses). The highly localized application of energy has led to more and more advanced rapid prototyping techniques such as laser sintering or stereolithography (Stampfl et al., 2004; Simchi, 2006).

Multi-photon polymerization (nPP, n = 2,3,…), in particular two-photon polymerization (2PP), has attracted continuously increasing attention after its first demonstration in 1997 as a method for the fabrication of three-dimensional structures with feature sizes far beyond the diffraction limit of the applied laser wavelength (Maruo et al., 1997; Tanaka et al., 2002). Contrary to conventional UV and (stereo-)lithography, 2PP is a truly three-dimensional laser writing technique. The underlying physical phenomenon of two-photon absorption (TPA) was theoretically postulated by Maria Göppert-Mayer in 1931 (Göppert-Mayer, 1931). It took, however, several decades to finally prove this effect due to the lack of highly irradiant light sources.

The invention of ultrafast lasers had led to many different applications. Particularly, the interaction of lasers with polymer surfaces and polymer or glass bulk samples is of high technological interest. The adaptation of polymers to laser beam characteristics and vice versa is very challenging from the scientific as well as from the technological point of view. Besides the implementation of two-photon absorption microscopy (Denk et al., 1990; Denk & Svoboda, 1997) and spectroscopy (Asaka et al., 1998; Yamaguchi & Tahara, 2003), TPA is

particularly used for the three-dimensional micromachining of a large variety of materials. Two- or multi-photon absorption processes are particular examples, in which focused ultrafast laser pulses are employed to trigger reactions in either glasses or photosensitive polymers (Cheng et al., 2003; Wong et al., 2006; Deubel et al., 2004). This technique uses the fact that TPA or nPA can only occur in the focal volume of the laser irradiation. Thus, the triggered reactions are strongly confined to the focal region, and the production of 3D microstructures is performed in one production step just by moving the focal volume in 3D through the materials. Among the applications of two-photon absorption so far are the fabrication of waveguides (Nolte et al., 2004; Houbertz et al., 2008a), of photonic crystal structures (Serbin et al., 2004; Houbertz et al., 2008b; Li et al., 2008), of phase masks (Jia et al., 2007), and the production of three-dimensional structures for medical applications such as scaffolds for regenerative medicine (Doraiswamy et al., 2005; Claeyssens et al., 2009; Beyer et al., 2010). Due to the possibility of creating *arbitrary* 3D micro- and macrostructures which are basically determined by the (shape/size of the) focal light intensity distribution of the focusing optics, other future applications will be conceivable which manifest themselves in the fact that the use of TPA processes for micromachining, microscopy, or spectroscopy is a continuously increasing field.

This chapter is organized as follows. First, general aspects of the material class of inorganic-organic hybrid polymers such as ORMOCER®s[1] will be described in order to give a brief overview about the materials and the accessible material parameters, followed by a brief description of selected materials for the TPA process. Then, the experimental setup which was used to fabricate small- and large-scale structures is described in detail. This section is followed by the characterization of two-photon absorption cross-sections of selected photoinitiators for the TPA processing. Finally, selected examples are given, ranging from the determination of voxel sizes in dependence of the laser parameters to high-resolution small-scale as well as large-scale structures (from sub-100 nm to the cm regime) fabricated by TPA. Future aspects of technology development will be addressed as well.

2. Inorganic-organic hybrid polymers

2.1 General material aspects

In order to combine the advantageous properties of inorganic and organic materials, different synthesis strategies are reported to produce inorganic-organic materials, ranging from physically blending organic materials with inorganic compounds via multi-step syntheses to one-step synthesis (Wojcik & Klein, 1995; Haas & Wolter, 1999). Nanostructured materials such as inorganic-organic hybrid polymers (ORMOCER®s) are intensively investigated due to their wide range of physical and chemical properties, synergistically resulting from their hybrid structure. The material concept of ORMOCER®s comprises the combination of material properties of organic polymers such as toughness, functionalization, and processing at low temperatures, with those of glass-like materials like hardness, chemical and thermal stability, and transparency on a molecular level (Haas, 2000). This concept allows one to achieve material properties which are not simply accessible with composite or polymer materials and, simultaneously, to apply various technologies to fabricate structures and elements on a different size scale. Due to the fact

[1]Registered trademark of the Fraunhofer-Gesellschaft für Angewandte Forschung e.V.

that the material properties of ORMOCER®s can be tailored as required by the respective applications, a large variety of different structures for applications in optics, ranging from the nm to the cm regime, in microelectronics, or in micro- and biomedicine is enabled. As the range of applications has been increased, the requirements on the materials and their processing have become more challenging, and the fabrication of microstructures with nm precision is a prerequisite for optical elements. Not only due to their excellent optical and electrical properties, but also due to their enhanced thermal, mechanical, and chemical stability and, simultaneously, their simple processability, they overcome the restrictions of purely organic polymers for most applications. In addition, functionalization is used to create suitable binding sites, particularly for biomolecules and cells for enabling micro- and biomedical applications.

Contrary to class-I hybrids, the material class of ORMOCER® consists of materials, where the inorganic and organic components are covalently bonded to each other (Sanchez et al., 2005). Their synthesis is carried out via catalytically controlled hydrolysis and (poly)condensation reactions using differently functionalized alkoxysilanes. Upon synthesis, an organically modified inorganic-oxidic network is established on a molecular level (Haas & Wolter, 2001), whereas also hetero-elements such as, for example zirconium, aluminum or titanium can be introduced into the network for further tuning of the material properties (Haas & Wolter, 1999; Helmerich et al., 1994; Declerck, 2010). The resulting hybrid materials are storage-stable resins with negative resist behavior, i.e. an organic cross-linking can be initiated via photochemical and/or thermal reactions.

The organic groups are employed as network modifiers, connecting groups, and also organically polymerizable moieties (cf., Figure 1). The latter are chosen with respect to application requirements. For example, for patterning via UV or laser lithography, (oligo-) methacrylate, acrylate, or styryl moieties are favored. Epoxy groups are preferred for thermal cross-linking in screen-printing processes. Alkyl or aryl groups as non-reactive groups can be connected to the –$[Si\text{-}O]_n$- network, and they also influence the material properties. An increase of their amount within the hybrid polymer can reduce the degree of polymerization due to sterical reasons, thus resulting in a reduced density in the coated layers. This directly influences the optical or dielectric properties such as the refractive index or the dielectric permittivity.

By varying the type and/or amount of alkoxysilane precursors and, in addition, the synthesis conditions (for example, the reaction temperature, the type and amount of catalyst, and/or the type and amount of solvent), custom-designed hybrid materials with a well-defined parameter profile can be provided for a large variety of applications. Among those are ORMOCER®s for microsystems which are applied, for example, as optical interconnects or waveguides (Streppel et al., 2002; Uhlig et al., 2006), in microoptics (Bräuer et al., 2001; Houbertz et al., 2006), in electro-optical applications (Robertsson et al., 1998; Houbertz et al., 2008a), as dielectric layers (Haas et al., 2006), and as passivation materials for the encapsulation of microelectronic devices and components (Houbertz et al., 2001; 2003a; 2003b).

The processing of an ORMOCER® typically consists of two steps. First, an organically modified -$[Si\text{-}O]_n$- network is established via chemical syntheses, resulting in a pre-polymer sol (resin). Second, the organic cross-linking is initiated photochemically and/or thermally which finally results in the formation of an inorganic-organic hybrid network. For that, UV and/or thermal initiators have to be introduced into the pre-polymer resin.

In Figure 1, a schematic sketch of selected multifunctional precursors which are employed for material synthesis is shown. In addition, some material properties being influenced by the individual precursors are summarized as well. As mentioned above, the hybrid polymers' material properties can be adjusted in wide ranges with respect to application via photochemical and / or thermal reactions. It has to be mentioned, however, that a change in one material property also might influence other material properties, and a comprehensive know-how is necessary to control this in a well-defined manner.

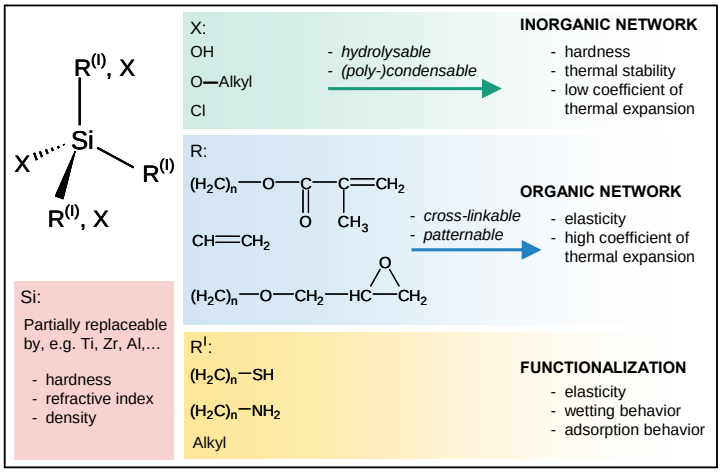

Fig. 1. Multifunctional precursors for ORMOCER® synthesis and their influence on resulting material properties.

For optical applications such as single- or multi-mode waveguides for the near infrared (NIR), the amount of Si-OH groups has to be as low as possible in order to reduce the materials' optical absorption losses which are basically determined by the amount of silanol groups due to 2nd harmonic (overtone) absorption at around 1438 nm (Rousseau & Boutevin, 1992). To the same extent, the materials' SiO_x content which intrinsically has a low optical loss is increased. It should be mentioned, however, that the higher the inorganic content, the more brittle the material will be, and the resulting layer thicknesses will also be reduced compared to a more organic material. The reduction of silanol groups can be performed, for example, by reducing them in the material by silylating agents, or by special synthesis conditions which are reported elsewhere (Buestrich et al., 2001). The best suited material for waveguide application should have no detectable –OH signal in multi-nuclei magnetic resonance (NMR) spectra. In addition, the amount of aliphatic -CH which is known to absorb around 1310 and 1550 nm was reduced in some ORMOCER®s to a minimum by increasing the amount of aromatic organic substituents. Scattering from the organically functionalized inorganic oligomers (polysilsesquioxanes) is not very likely, because their structural size, which was determined by small angle X-ray scattering (SAXS) measurements, is in the range from 1 to 3 nm for ORMOCER®s applied in optics. The structural features of the hybrid polymers are dependent on the precursors which are used for synthesis. For example, by NMR spectroscopy it can be shown that di-alkoxysilanes yield chain or ring polymers, while tri-alkoxysilanes can result in three-dimensional networks.

The mechanical properties of ORMOCER®s can be also varied over a wide range (Haas & Wolter, 1999). For example, the Young's modulus and the mechanical and thermal stability can be increased by increasing the inorganic content in the hybrid network. This simultaneously leads to a reduction of the coefficient of thermal expansion (CTE). Solvents which are produced upon syntheses are usually removed from the hybrid polymer resins in order to allow either solvent-free processing, or to replace them by other solvents or reactive diluters. This provides highest flexibility in thin-film processing, because the materials' viscosity can be simply adjusted to the process requirements. The storage stability with and without photoinitiators was characterized for selected ORMOCER® materials to be more than two years at room-temperature. For a prolonged storage, the materials should be kept at 4 or -18 °C, respectively.

2.2 Selected materials for TPA processes

For the TPA experiments, three different hybrid polymer modifications were chosen with respect to their reaction reactivity which significantly differs for each material. These ORMOCER®s are typically applied in optics and for biomedical applications. As reactive moieties, either acrylate, (oligo-)methacrylate, or styryl groups were chosen. The photochemical reactivity of acrylate groups in the TPA process is usually much higher than the one of methacrylate or styryl groups, thus resulting in higher reaction rate.
The materials were modified such that their response to the femtosecond laser pulses is very high in order to achieve a high densification of the laser light-exposed areas. Several chromophore and initiator systems, respectively, were used to radically initiate the organic cross-linking by TPA. Their concentration in the ORMOCER® materials was set to be between 0.05 and 3 wt.-%. However, the two-photon absorption cross-section σ_2 of these chromophores and initiators was reported in the literature to differ significantly, being as low as approximately 10^{-55} cm^4s (10^{-5} GM) for 2-benzyl-2-dimethylamino-4'-morpholinobutyrophenone (Serbin et al., 2003), or as high as $1250 \cdot 10^{-50}$ cm^4s (1250 GM) (Cumpston et al., 1999; Schafer et al., 2004). All selected materials are transparent for the laser wavelength, showing absorption losses of about 0.02 to 0.04 dB/cm.

3. Multi-photon patterning

3.1 General aspects

Multi-photon polymerization (nPP) processes are used to realize arbitrary three-dimensional structures without any complicated processing sequences by multi-photon absorption (nPA) in various materials such as, for example photosensitive materials. Typically, two-photon absorption processes are considered due to their higher process probability compared to higher order processes, and they are used to trigger the materials' organic polymerization by photochemical reaction with ultra-short laser pulses (Maruo et al., 1997; Tanaka et al., 2002; Houbertz et al., 2007; 2008a; 2008b; Jia et al., 2007; Li et al., 2008). Particularly, the 3D patterning of hybrid polymers such as ORMOCER®s is of high technological interest for application in optics or biomedicine.
Due to the threshold behavior and the non-linear nature of the nPP process, structures far beyond the diffraction limit can be achieved by choosing a suitable combination of pulse energy, number of applied pulses, material, and initiator system (Tanaka et al., 2002; Steenhusen et al., 2010a; 2010b). This technique uses the fact that TPA only occurs in the

focal volume of the laser irradiation, where the photon density is locally high enough to initiate TPA, while the entire material has to be transparent for the laser wavelength. Thus, the organic cross-linking of the material is strongly confined to the focal region, enabling the computer-assisted fabrication of 3D microstructures in only one production step just by moving the focal volume through the ORMOCER® material in x, y, and z direction.

3.2 Experimental setup

In Figure 2, a principal sketch of the experimental setup for nPP patterning is shown which is used for small- and large-scale patterning of ORMOCER®s. The setup consists of a laser and a second harmonic generation (SHG) system, an acousto-optical modulator (AOM), and three air-bearing motion stages for the 3D movement of the sample and the optics, respectively. While most setups employ Ti:sapphire laser systems operating at 780 to 800 nm for the processing of polymer or hybrid polymer materials (Tanaka et al., 2002; Houbertz et al., 2008a; 2008b; Doraiswamy et al., 2005; Claeyssens et al., 2009; Schizas et al., 2010; Gittard et al., 2010), the laser system in the present setup emits at a fundamental wavelength of 1030 nm. This is converted to visible light for the 2PP process by SHG. Three-photon polymerization (3PP) processes are initiated at the fundamental wavelength, i.e. without using SHG.

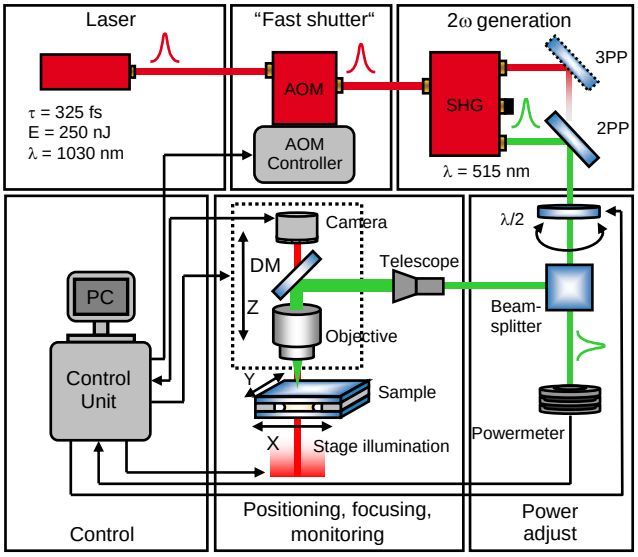

Fig. 2. Experimental setup for multi-photon polymerization (nPP) for the fabrication of 3D structures. DM: dichroic mirror, AOM: acousto-optic modulator.

The laser is a diode-pumped low-cost Ytterbium-based femtosecond laser system. The pulse duration is about 325 fs at 1030 nm (determined for 2.3 W). The lasers' repetition rate is 10.1 MHz, and the maximum pulse energy is 230 nJ. A combination of polarizing beam splitter and half-wave plate mounted on a computer-controlled rotary stage (Aerotech ADR 160) allows a well-defined control of the pulse energy. The acousto-optical modulator (AOM) which is also computer-controlled is used for switching the laser light on and off. All reported average powers were determined below the focusing microscope objectives.

For the 2PP patterning, the 515 nm (SHG) irradiation is expanded by a factor of three before being focused into the ORMOCER®. The focusing is carried out using a microscope objective with a numerical aperture (N.A.) of 1.4 for the fabrication of small-scale structures (up to approximately 100 µm in height) (Steenhusen et al., 2010a), and with either a Nikon CFI Super Plan Fluor ELWD 40XC objective with an NA of 0.60 or a Nikon CFI Super Plan Fluor ELWD 20XC objective with an NA of 0.45. Both of the latter have long working distances of about 3.8 mm and 8.2 mm, respectively, for the creation of large-scale structures (up to 1 cm) (Stichel et al., 2010). For the 3D movement of sample and optics, an Aerotech ABL-1000 three axis system is used with a travel distance of 10 cm x 15 cm x 15 cm in x, y, and z direction, respectively. The setup allows scanning speeds up to 300 mm/s which is useful for the fabrication of larger structures, and a precision of a few nanometers for the generation of high-resolution structures. The patterning can be monitored in-situ by illuminating the sample with red light from the backside, and detecting the transmission with a CCD camera placed behind a dichroic mirror (DM).

The hybrid polymer resin is dispensed on glass substrates. Dependent on the required structure sizes, the patterning is carried out using different exposure strategies which are depicted in Figure 3. For small-scale structures, two standard setups are used. In one setup, the material is sandwiched between two glass substrates, separated by a distance holder (approximately 100 µm in thickness; cf., Figure 3 (a)). In the second setup, the material is deposited as a droplet, being located head first on a glass substrate (Figure 3 (b)). Subsequent cross-linking in order to generate the complete 3D structure is then performed

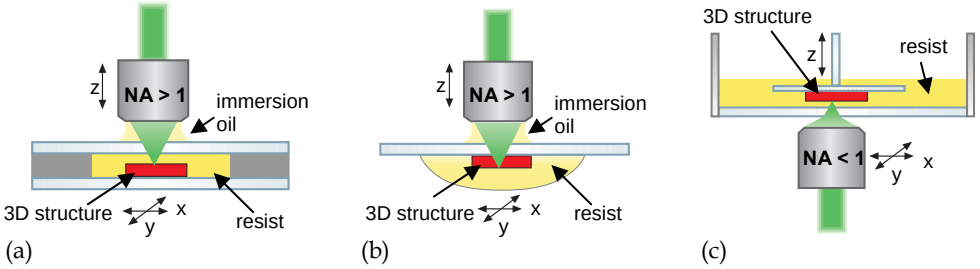

Fig. 3. Exposure strategies. For high-resolution patterning, the material is placed (a) between two glass plates separated by a distance holder, or placed (b) as droplet head first. (c) For large-scale fabrication, an inverted setup is used with a material bath, a sample holder, and an objective scanning the x-y-plane below the bath.

by moving the focus through the resin. In both cases, the structure is then built up starting at the glass substrate's surface. However, in the first case, patterning is carried out by moving the pulsed laser beam up through the hybrid polymer's volume, while for the second setup the patterning is performed through the volume of the already cross-linked material. It has to be mentioned that beam distortion might occur for the setup displayed in Figure 3 (b) due to the fact that the light has to travel trough the already cross-linked material, having a higher refractive index than the liquid resist. Finally, for very large-scale structures, the setup is inverted, using a bath as material reservoir, a sample holder movable in the z direction, and an x-y-scanning objective. The sample is moved upwards which enables one to build structures whose heights are not limited by the working distance of the employed objective anymore.

Contrary to other lithography methods such as conventional UV or laser lithography, the 2PP process can be carried out also in the volume of the materials. Thus, principally two types of processes can be performed which are schematically depicted in Figure 4. On the one hand, the patterning process can be carried out, initiating a cross-linking of the materials' photochemically active organic moieties, followed by a subsequent removal of the non-exposed parts in a suitable developer solvent, analogously to classical processing schemes (solvent-based processing, Figure 4 (a)). On the other hand, structural features can be written inside the hybrid resins' volume, while the surrounding material is not removed by a developer, and which can be differently treated in further processing steps (solvent-free processing, Figure 4 (b)) (Houbertz, 2007; Houbertz et al., 2008). Examples for both routes will be given in chapter 3.4.

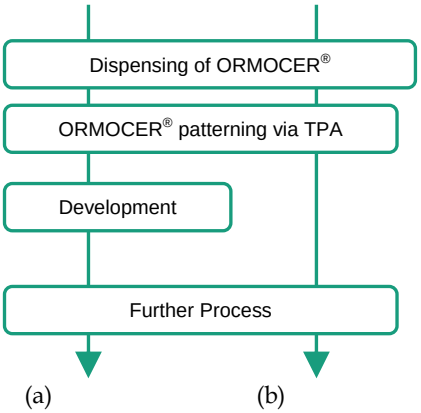

Fig. 4. Process flow diagram. (a) Solvent-based, and (b) solvent-free processing.

3.3 Absorption cross-sections

In order to characterize the non-linear properties of the photoinitiators which are introduced into the selected ORMOCER® materials, a z-scan experiment was set up which determines the transmitted laser light signal passing a quartz glass cuvette filled with initiator/solvent solution. It is widely accepted that the higher the initiators' absorption cross-sections, the more efficient should be the TPA process. It should be mentioned, however, that not only the absorption cross-section of the employed photoinitiators determine the process efficiency, but also the surrounding matrix, i.e. ORMOCER® material and solvents, if included. The latter two might have a much stronger influence on the process efficiency than the absorption cross-section of the initiators itself (Houbertz et al.; 2010).

There are two effects which can occur, namely non-linear absorption and non-linear refraction, and which were theoretically described in literature (Sheikbahae et al., 1989; Sheikbahae et al., 1990). Non linear refraction causes a phase shift of the incident laser beam depending on the irradiance, because the materials' refractive index also varies with irradiance. This is the reason why the incoming beam in a z-scan experiment is focused and defocused, if the cuvette is scanned across the focal region. Due to the fact that nPA is dependent on the irradiance at the sample, the transmitted signal will have a dip for the sample being directly located in the focus. From the magnitude of this dip, the TPA cross-section σ_2 can be calculated (van Stryland & Sheikbahae, 1998).

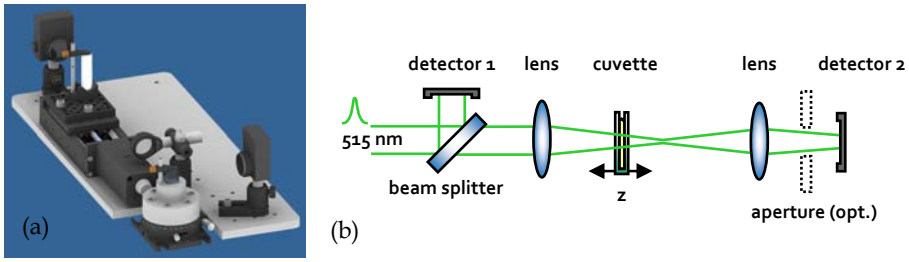

Fig. 5. Experimental setup for the z scan. (a) 3D view, and (b) schematic sketch of the setup.

In Figure 5, a 3D presentation of the experimental setup for the z-scan experiment as well as a schematic sketch is shown which was used to determine the TPA absorption cross-sections of the photoinitiators. As laser wavelength, 515 nm pulses were used which were split with a beam splitter for providing reference and transmission signal. The transmitted beam is then focused using a lens, and detected with a 9.8 mm photodiode (detector 2). Optionally, a variable aperture and an additional lens are located in front of the photodiode. The photoinitiators were dissolved in methylisobutylketone in a 1 mm quartz glass cuvette which is moved along the beam propagation path with a 75 mm linear travel stage. The signal-to-noise ratio was improved by recording multiple scans for each measurement.

For the determination of the absorption cross-sections, non-linear refraction should be neglectable. This can be achieved by an open-aperture scan, where the transmitted signal only depends on the non-linear absorption which is dominated by TPA. The fraction of non-linear refraction can be determined by using the aperture in front of the detecting photodiode, resulting in additional signals in the transmission curve (Sheikbahae et al., 1989).

Aside a high absorption cross-section of the photoinitiators, a high chemical reactivity of the hybrid resins is required. A first insight into their reactivity in selected hybrid polymer systems was deducted from photo-DSC (photo-differential scanning calorimetry) measurements of the ORMOCER®/initiator formulations. It has to be mentioned, however, that the underlying reaction is initiated in a classical one-photon process which already gives a good measure of the reaction enthalpy, and thus of the materials' cross-linking behavior upon UV light exposure. From these measurements, two different commercially available UV initiators were chosen, henceforth labeled as Ini1 and Ini2 (BASF), respectively, as well as a specially developed photoinitiator, labeled as Ini3 (Seidl & Liska, 2007).

In order to prove whether non-linear absorption and/or non-linear refraction are taking place, the magnitude of the absorption dip was determined in dependence of the excitation power. The result is shown in Figure 6 (a). For pure two-photon absorption, a linear power dependence with no offset is expected from the theory (equation (1)). For the exclusion of non-linear refraction, the transmission measurements were repeated with an additional lens and aperture placed in front of detector 2 (cf., Figure 5). If there is no influence on the transmission signal upon opening and closing the aperture, the detector area is large enough, and defocusing attributed to non-linear refraction can be neglected. In Figure 6 (b), a representative z-scan transmission curve is shown. The curve was recorded using a solution of Ini3 and MIBK at an average laser power of 243 mW.

According to the theory (van Stryland & Sheikbahae, 1989), the change in the transmission is given by

$$\Delta T(z) = \frac{\alpha_2 I_0}{2\sqrt{2}} \cdot \frac{1-\exp(-\alpha_1 L)}{\alpha_1} \cdot \frac{1}{1+z^2/z_R^2} \quad , \tag{1}$$

with α_1 and α_2 as linear and non-linear absorption coefficients, respectively, and z as the cuvette position. z_R is the Rayleigh length, and L is the sample thickness. The intensity I_0 is proportional to the average laser power.

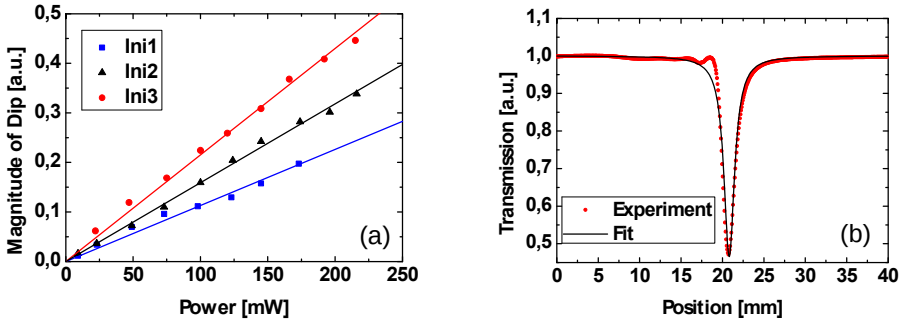

Fig. 6. z-scan results. (a) Magnitude of the transmission signal dip as a function of excitation power for three different photoinitiators. (b) Open aperture trace for Ini3 (for better illustration, only every fifth point is shown).

Due to a negligible linear absorption coefficient, the second term in equation (1) can be approximated by the sample thickness L, leading to a more simplified expression. The non-linear absorption coefficient α_2 can be correlated to the TPA cross-section σ_2 using the photon energy and the density of the initiator molecules in the cuvette. In addition, information on the beam waist w_0 is necessary for the determination of the incident on-axis irradiation I_0. This was determined with a home-built USB camera beam profiler which was scanned along the beam path. A beam waist of about 16 µm was found for the underlying focusing conditions, i.e. the thin sample approximation $z_R > L$ is valid (Sheikbahae et al., 1989).

The TPA cross-sections can be better determined from the slopes of the curves in Figure 6(a), which yield better statistics, because more measurements contribute to the determination of σ_2. From the data it was calculated that Ini3 has the highest absorption cross-section, and thus the highest TPA efficiency, followed by Ini2, while Ini1 has the lowest absorption cross-section which is about a factor of 10 lower than published for the same initiator by Schafer et al. (Schafer et al., 2004). The quantitative results are summarized in Table 1.

Initiator / Cross-section	Ini1	Ini2	Ini3
σ_2 (m^4s)	$(6.7 \pm 0.4) \cdot 10^{-59}$	$(1.4 \pm 0.3) \cdot 10^{-58}$	$(3.2 \pm 0.2) \cdot 10^{-56}$
σ_2 (GM)	0.7	1.4	320
σ_2 (relative to Ini1)	1 ± 0.1	2.1 ± 0.4	472 ± 32

Tab. 1. Calculated TPA cross-sections for Ini1, Ini2, and Ini3. The error bars were determined by identifying the minimum and maximum slope found for each photoinitiator.

There are several possible explanations for the difference in σ_2. The presence of non-linear refraction which significantly influences the TPA cross-section results towards higher

values, and cannot be excluded in the data of Schafer et al. (Schafer et al., 2004) due to the fact that no details are given in their publication. Finally, the determination of the beam waist w_0 is difficult and a significant source of error in the determination of σ_2. This is related to the quadratic dependence of I_0 on w_0, i.e. only slight deviations in w_0 will significantly impact the value of σ_2. Therefore, Table 1 also gives relative absorption cross-sections (normalized to Ini1) in order to allow a better comparison of the different photoinitiators.

3.4 TPA patterning

3.4.1 TPA-written arbitrary 3D structures

The most impressing way of demonstrating the possibilities of TPA processing is to write computer-generated, arbitrary 3D structures which demonstrate the ability of scaling up structures from the µm to the cm scale. In order to show the power and the beauty of the technology, we have produced various 3D microstructures using differently functionalized ORMOCER® materials with two commercially available initiators (Ini1 and Ini2, alternatively). Figure 7 shows examples of arbitrary 3D structures which were fabricated in an acrylate and a methacrylate-functionalized ORMOCER®, henceforth labeled as OC-V and OC-I, respectively.

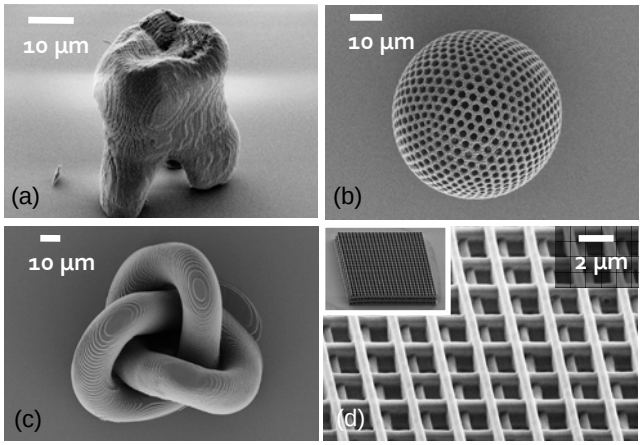

Fig. 7. Selected 3D structures, fabricated by 2PP for different ORMOCER® formulations. (a) Tooth created in OC-I/Ini1 [average power: 500 µW, dimensions: (32 x 37 x 55) µm³], (b) Hollow ball after (Hart,2009) written in OC-V/Ini2 [average power: 34 µW, diameter: 75 µm, hatch distance: 500 nm], (c) Knot after (Wei,2010) created in OC-V/Ini2 [average power: 105 µW, dimensions: (90 x 90 x 50) µm³]. (d) Photonic crystal structure after (Steenhusen, 2008) written in OC-V/Ini1 [average power: 48 µW, period of 2 µm, dimensions: (50 x 50 x 6) µm³]. The writing speeds were (a), (c) 50, (b) 100, and (d) 60 µm/s. All materials were formulated with 3 wt.-% photoinitiator except for (c) which includes only 1 wt.-% initiator.

3.4.2 Voxel size determination

While these types of structures typically inspire end-users, only little is known about the cross-linking behavior of hybrid polymers in this process due to the fact that many effects

influence the reaction kinetics. The minimum achievable feature sizes are related to different effects, which occur simultaneously in the 2PP experiment, influencing each other and which finally will determine the voxel size. Among them are the diffusion of initiators and oxygen molecules, the polarity of the ORMOCER® matrix or traces of solvents, and the process efficiency of the photoinitiator, only to mention some. It could be shown by Monte Carlo simulations that initiator molecules spread into free space after being excited by one or several laser pulses. According to this diffusion of initiator radicals, the voxel is enlarged significantly, because polymerization can be triggered outside the focal volume (Steenhusen, 2008). Oxygen which is present in each material is known to act as radical scavenger, i.e. upon formation of initiating radicals by (laser) light irradiation the initiator's triplet states will, for example be quenched, thus reducing the amount of initiating radicals in the resin (see, e.g. Studer et al., 2003). Although it is widely accepted that the TPA efficiency of the photoinitiators plays a major role in the initiation of the cross-linking, the matrix materials which contain these initiators as well as the propagation of chain growth and termination reactions also have significant impact on the reaction kinetics (Houbertz et al., 2010).

Thus, the voxel dimensions are not only dependent on the technical equipment such as optics used for patterning. Figure 8 shows a schematic of the different interaction volumes which influence the minimum voxel dimensions in TPA-initiated cross-linking experiments, impacting the resulting feature sizes significantly.

The technical interaction volume (red in Figure 8) is principally determined by the employed optics, by the stability of the laser, and by the stability and accuracy of the positioning system. From a technical point of view, this can be optimized by using specially adapted optics (Fuchs et al., 2006), by stabilizing the laser source, and by employing highly accurate positioning stages, mounted on suitable damping systems. The chemical interaction volume (green in Figure 8), however, is much more complicated to minimize, because this is dependent on many different factors such as, for example by the reaction kinetics of the material formulation and, consequently, on the laser-light initiated propagation and termination reactions in the hybrid resin, as already described above. In addition to them, the reaction rate is also influenced by the diffusion of radicals and radical scavengers in the liquid resin (Steenhusen, 2008; Struder et al., 2003).

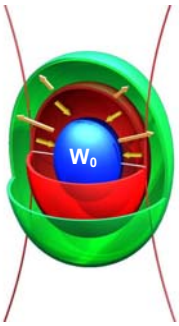

Fig. 8. Schematics of the different interaction volumes, influencing the achievable voxel sizes in a 2PP experiment: technical (red) and chemical (green) interaction volume. The threshold behavior determines the third interaction volume (blue).

The third effect, i.e. the threshold behavior (blue in Figure 8; Tanaka et al., 2002) of the reaction, could principally lead to infinitesimal small voxel sizes. However, aside the exposure dose (determined by the average power, the number of pulses, and the writing speed), the threshold behavior is also dependent on the minimum initiator (i.e. the threshold) concentration necessary to start the chemical reaction. This, however, is not really known, and thus not as well-defined as the laser parameters.
In order to gather information on the 2PP process for a given material formulation, voxel arrays were written using the ascending scan method which is described elsewhere (Sun et al., 2002). In Figure 9, a voxel array is shown which was written using a constant average power of 164 µW. From the left to the right, the exposure time was varied in 2.5 ms intervals, and the height of the laser focus was varied in intervals of 0.25 µm from the top to the bottom of the array. The voxel pitch was set to 2 µm. It has to be mentioned, however, that the degree of cross-linking also has to be considered which will be discussed in the next section.

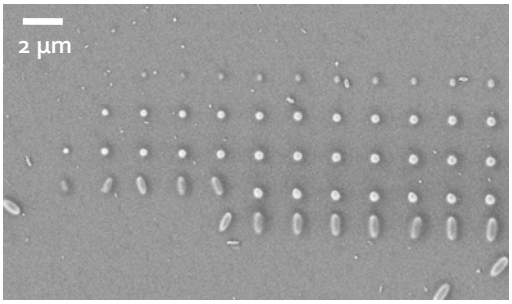

Fig. 9. Typical voxel field created in OC-V with the ascending scan method (Steenhusen et al., 2010a).

Contrary to 2PP experiments previously reported (Kawata et al., 2001; Serbin et al., 2003), the pulse energy for initiating a photochemical reaction is much lower in the present case, being only about 5 to 50 pJ, under the assumption that the focusing condition and the writing speed are comparable in the experiments. There are two possible reasons for this which will be briefly summarized in the following. First of all, the literature data were created using a central wavelength of 800 nm which is about 30 % higher than the wavelength used for our experiments. The overlap of the initiators' maximum in linear extinction coefficient with the laser spectrum significantly determines the process efficiency (Houbertz et al., 2006). For the chosen initiators, this overlap is much more pronounced at 515 than at 800 nm. In addition, a specially designed acrylate-based ORMOCER® system was used for the experiments which usually has a much higher reaction rate than, for example methacrylate-based materials (Odian, 1981).

3.4.3 Investigation on voxel sizes

In order to account for a well-defined fabrication of 3D functional structures for application, an understanding of the underlying polymerization processes initiated by the laser light/material interaction is necessary. By Serbin et al. (Serbin et al., 2003), a simple model which can be used in a first approximation for estimating the voxel diameter d was proposed, where d is given by

$$d(t,F_0) = w_0\sqrt{\ln\left(\frac{\sigma_2^* F_0^2 t\nu\tau}{\ln(\rho_0/\rho_0-\rho_{th})}\right)}. \quad (2)$$

However, the beam waist w_0, the effective TPA cross-section σ_2*, and the threshold radical concentration ρ_{th} for the initiation of the 2PP process which are needed for the calculation of the voxel diameter are not known. The initial photoinitiator concentration is given by ρ_0, F_0 describes the incident photon flux, and t, ν, and τ are the temporal parameters exposure time, repetition rate, and pulse duration, respectively.

In order to investigate the 2PP process at 515 nm, exactly the same material formulation as reported by Serbin et al. was used to create voxel arrays (Steenhusen et al., 2010a). The average laser powers at which voxels could be fabricated were three orders of magnitude lower than reported in (Serbin et al., 2003), i.e. in the µW instead of the mW regime. From the data evaluation assuming the same threshold radical density of 0.25 wt.-%, a TPA cross-section was determined which is four orders of magnitude higher than the one given by Serbin et al.. These differences in the 2PP process are attributed to the higher overlap of the laser spectrum with the initiators' extinction spectrum, because the chemical composition in both experiments is the same.

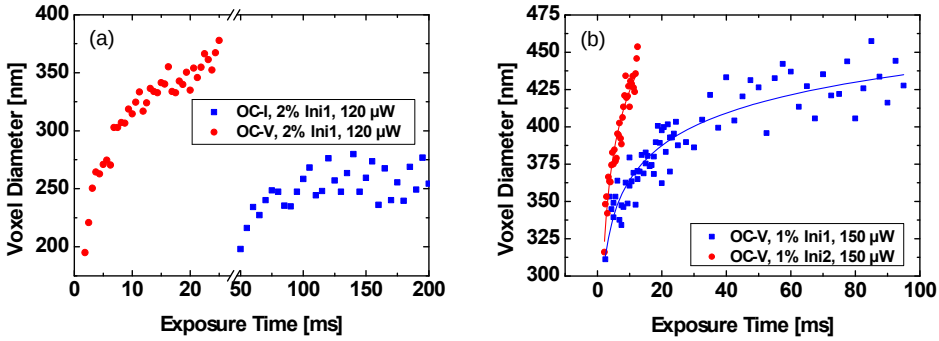

Fig. 10. (a) Voxel size dependence on the applied exposure time for OC-I and OC-V, both formulated with 2 wt.-% Ini1 at an average laser power of 120 µW. (b) Impact of the initiator on the voxel size of OC-V, formulated with 1 wt.-% of Ini1 and Ini2 (Steenhusen et al., 2010a).

In order to demonstrate the different reactivity of various ORMOCER® material systems, voxel arrays were written using OC-I and OC-V, both formulated with 2 wt.-% Ini1, and the resulting voxel diameters were evaluated. In Figure 10 (a), the voxel diameters determined from voxel arrays generated in acrylate-based (OC-V) and the methacrylate-based (OC-I) ORMOCER®s are compared. Obvious from the data is that OC-V requires a significantly shorter exposure time (and thus exposure dose) in order to produce a voxel equivalent in size of the ones fabricated in OC-I which is related to the different reaction rates of acrylate and methacrylate groups (Odian, 1981). A comparison of the TPA cross-sections, however, cannot be performed, since the threshold concentrations will significantly differ due to the different cross-linkable moieties. In addition, the materials have different polarity as well as different oxygen sensitivity.

The voxel diameters of OC-V in dependence of the exposure time are compared. The material was formulated with two different photoinitiators of the same concentration (1 wt.-% Ini1 and Ini2, respectively, at an average laser power of 150 µW). The results are shown in Figure 10 (b). For the formulation of OC-V with Ini2, the voxel diameter increases much steeper than for the same material formulated with Ini1, i.e. Ini2 is much more efficient. From the fits using the model of (Serbin et al., 2003), the TPA cross-section of Ini2 is approximately two times larger than the one of Ini1, which is in good agreement to the z-scan data (cf., Table 1; Steenhusen et al., 2010a). A more comprehensive study will be published elsewhere.

The effect of different initiator concentrations on the voxel formation was also investigated for OC-V at a given average laser power and varying the exposure times which is reported elsewhere (Steenhusen et al., 2010a). Beside other findings, it was observed that the dependency of the voxel sizes on the initiator concentration is not linear. From investigations on the cross-linking behavior and the resulting refractive indices in dependence of the UV initiator concentrations which were carried out by one-photon processes (classical UV exposure), it was concluded that different initiator concentrations lead to different inorganic-organic hybrid networks in the final layer (Houbertz et al., 2004; Fodermeyer, 2009; Landgraf, 2010).

Finally, the extraordinary performance of Ini3 should be underlined by the fact that voxel sizes comparable to the ones fabricated using Ini1 and Ini2 in a given ORMOCER® material system were achieved with an about 200 times lower initial initiator concentration of Ini3 than of Ini1 or Ini2.

An investigation of the voxel diameter in dependence of the exposure time at different average laser powers has revealed that the higher the laser power, the larger the voxel diameters will be (Steenhusen et al., 2010a). The determined TPA cross-section σ_2 by using equation (2), however, are about two times larger than derived from the z-scan experiments, which can be attributed to the fact that the assumed threshold concentration of 0.25 wt.-% is too high. Additional experiments with conventional UV exposure which were carried out to support this statement have revealed that the organic cross-linking can be initiated for initiator concentrations being as low as 0.01 wt.-% (Landgraf, 2010). However, although the model proposed by (Serbin et al., 2003) yields a reasonable starting point for theoretically determining the TPA cross-sections, it lacks of some important effects such as the diffusion initiator radicals or molecular oxygen.

As mentioned above, the minimum voxel sizes which can be fabricated are dependent on many different parameters, among which the chemical and the threshold behavior are the most difficult to quantify. In the following, some results will be presented for sub-100 nm patterning, and they will be discussed with respect to the degree of organic cross-linking.

The typical minimum feature sizes reported for several years were about 100 nm ("resolution limit"). Recently, several groups have reported sub-100 nm resolution using various polymer materials, where minimum feature sizes down to 40 nm were achieved, some of them using the stimulated emission depletion (STED) approach (Li et al., 2009; Andrew et al., 2009; Haske et al., 2007). In Figure 11, a representative image of a voxel, fabricated in a styryl-based ORMOCER®, formulated with 2 wt.-% Ini1 is shown. The patterning was carried out at an average laser power of 65 µW and an exposure time of 100 ms, with no further optimization of the technical equipment, yielding a voxel diameter of about 90 nm. Features as small as about 75 nm can be routinely achieved, and the data will routinely achieved, and these data be published elsewhere.

From conventional UV lithography in dependence on the processing parameters it is known that the organic cross-linking is very sensitive to the process conditions. If these are not suitably chosen or adapted, part of the material will not be cross-linked, and will be removed in the development step. This then results, for example in lower layer thicknesses or smaller structures than adjusted. The same effects can be observed in 2PP experiments, since the underlying process is a laser light-induced organic cross-linking, i.e. if the 2PP parameters are not optimized with respect to the reaction kinetics of the material, smaller structures consequently will result. It has to be mentioned, however, that there is a trade-off between threshold effect and cross-linking by reducing the photon dose. By driving the threshold effect, smaller structures will definitely occur which, however, might not be as well cross-linked as voxels being fabricated with a higher photon dose and/or initiator concentration, i.e. the resulting voxels will be less stable, and further reduction in size by the development step might thus occur. This needs to be investigated in more detail.

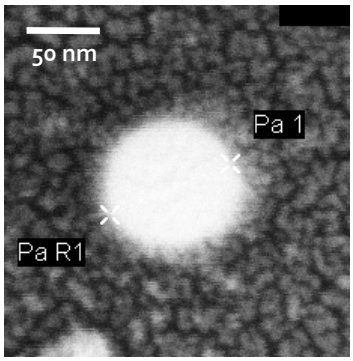

Fig. 11. Sub-100 nm voxel (diameter: 90 nm), fabricated by 2PP in a styryl-based ORMOCER® material, formulated with 2 wt.-% Ini1.

We therefore have started to investigate the degree of organic cross-linking of ORMOCER® materials which were processed by 2PP by high-resolution µ-Raman spectroscopy. In Figure 12, typical µ-Raman spectra are displayed as well as the degree of organic cross-linking of OC-I formulated with 1 wt.-% Ini1 in dependence on the average laser power. As µ-Raman sample, squares of 10 µm x 10 µm were written with a velocity of 100 µm/s and a hatch distance of 0.1 µm. In Figure 12 (a), two µ-Raman spectra are displayed for a different cross-linking state of OC-I. At about 1648 cm^{-1}, the C=C bond resulting from the methacrylate groups which decreases in intensity the more cross-linked the material is can be seen. As internal reference, the C=C bond of the diphenylsilane precursor at 1569 cm^{-1} was used. The calculation of the degree of cross-linking was performed as reported in (Houbertz et al., 2004), and the first result is shown in Figure 12 (b). Analogously to the results from ORMOCER® layers which were prepared by conventional UV lithography, the degree of cross-linking increases continuously until saturation for the given process conditions. However, almost the same magnitude in organic cross-linking is achieved in saturation by TPA processing as for classical UV exposure. A more comprehensive study on the TPA-initiated organic cross-linking will be published elsewhere.
Additionally to the 2PP experiments, first patterning by 3PP using the fundamental wavelength of 1030 nm was performed which was straightforward when considering the

extinction spectra of the initiators (Steenhusen et al., 2010a). From the spectra it can be concluded that no TPA processes will occur, because there is no absorption of the initiator at 515 nm. Excitation with three photons, is likely depending on the three-photon absorption cross-sections which have to be evaluated for the different systems from z-scan experiments at 1030 nm. The latter is still under investigation. A resulting voxel array written using OC-1 with 2 wt.-% Ini1 and an exposure time of 200 ms is displayed in Figure 13. A photonic crystal structure written by 3PP can be found in (Steenhusen et al., 2010b).
The average laser power was with 5.2 to 5.7 mW about three orders of magnitude higher than for the respective TPA process at 515 nm, indicating a higher order non-linear process, being related to the lower efficiency of the 3PA process compared to the TPA process.

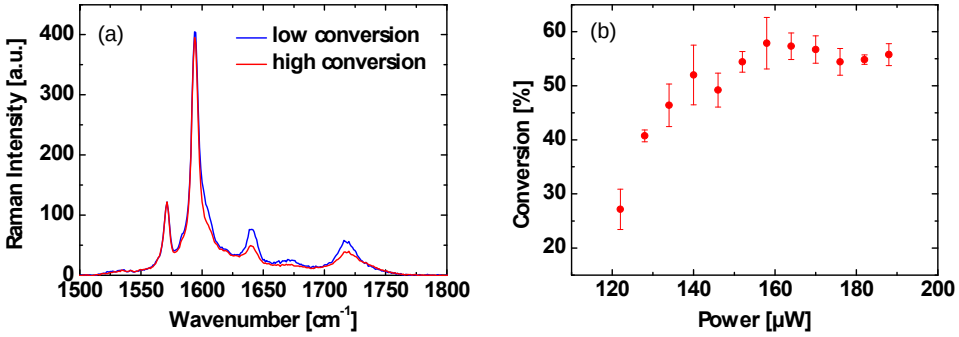

Fig. 12. Cross-linking investigations of OC-1/1 wt.-% Ini1. (a) Selected µ-Raman spectra, and (b) degree of organic cross-linking in dependence on the average laser power.

By evaluating the voxel size, it can be seen that features being only the seventh part of the fundamental wavelength are achieved. The voxel pitch was set to 2 µm, and the smallest voxel in these data has a diameter as low as 155 nm which is far beyond the diffraction limit. However, also for these data the degree of organic cross-linking needs further investigation in order to give final proof for real sub-diffraction limit structures.

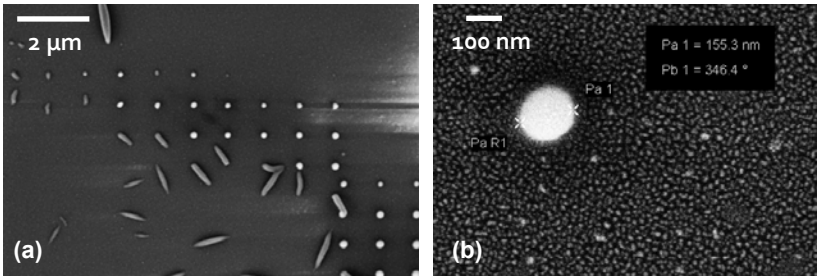

Fig. 13. (a) Voxel array (pitch 2 µm) written by 3PP in OC-1/2 wt.-% Ini1, and (b) zoom into (a), displaying an individual voxel of about 155 nm in diameter (i.e., a feature size of λ/7).

The data yield a proof of concept for 3PP experiments at 1030 nm. By varying the exposure parameters, a tremendous potential for further decreasing the feature sizes is seen. A more

comprehensive study of 3PP processes at 1030 nm including z-scan experiments is presently carried out, and will be published elsewhere.

3.4.4 Large-scale TPA patterning

Up to now, most patterning results making use of TPA processes are restricted to smaller scale structures, where typically structures of view hundreds of µm in size were reported (Ostendorf & Chichkov, 2006). The restriction in structure dimensions is mainly related to limitations of the working distance of the high-NA focussing optics and to long fabrication times. Instead of the focussing objective with an NA of 1.4 which is used for high-resolution patterning, for large-scale fabrication this objective was replaced either by a microscopy objective with an NA of 0.60 or with an NA of 0.45, characterized by long working distances (cf., section 2.2). In addition, they offer a correction collar enabling an adaptation to different cover glass thicknesses ranging between 0 and 2 mm in order to reduce spherical aberration, resulting from a refractive index mismatch of air, glass substrate, and ORMOCER® resin, leading to blurring of the focal light distribution. Due to fact that the refractive index mismatch of glass and resin is very small compared to their difference to the refractive index of air, the spacer thickness can be included into the corrective adjustments. Nevertheless, this correction of the spherical aberration is only valid for a distinct penetration depth of the focal spot into the resin, and thus inhomogeneous patterning results can be observed during processing with the common sandwich configuration (cf., Figure 3 (a)) and varying the penetration depth by vertically objective movement (Stichel et al., 2010).
In order to demonstrate the full potential of the TPA technology, the experimental setup for the TPA patterning was modified (cf., Figure 3 (c)) in order to allow the fabrication of high resolution large-scale structures with structure heights being not limited by the objective's working distance. These structures might be employed, for example as scaffolds for regenerative or biomedicine (see also section 3.4.5). In Figure 14, two examples for the 3D fabrication of arbitrary 3D large-scale structures by 2PP in an acrylate-based ORMOCER® (OC-V/2 wt.-% Ini2) are shown.

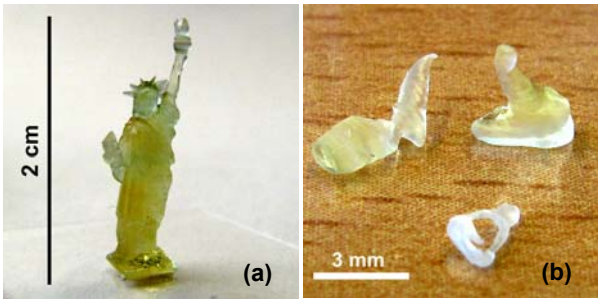

Fig. 14. Examples of large-scale structures fabricated by 2PP in OC-V, formulated with 2 wt.-% Ini2. (a) Statue of liberty, and (b) human ossicles in life-size.

3.4.5 Application examples

Finally, in this section two application examples will be given, one for optics and the other one for biomedical applications.

Due to the fact that the selected ORMOCER® materials exhibit particularly low absorption losses at data and telecom wavelengths (850, 1310, and 1550 nm) (Houbertz et al., 2003b), the employment of TPA for the fabrication of highly sophisticated optical designs would be advantageous, since this process can also be carried out on pre-configured substrates, already containing opto-electronic elements such as laser- or photodiodes, vertical cavity surface emitting lasers (VCSEL), or microlenses.
Two-photon absorption (TPA) processing was used for the fabrication of multimode waveguide (WG) using just one individual ORMOCER® material which was specially designed for the process. This reduces the process steps significantly, and only two to three process steps need to be performed in order to create the waveguide (Houbertz, 2007; Houbertz et al., 2008). The ORMOCER® material was coated onto a pre-configured printed-circuit board (PCB) substrate, where laser source (transmitter) and photo-diode (receiver) were already mounted. As laser source for this application, a femtosecond laser (fundamental wavelength λ = 800 nm, pulse durations between 130 and 150 fs) was employed, and focused about 80 to 250 µm deep into the ORMOCER® layer without using a cover glass. This depth is just dependent on the position of the optoelectronic devices' active surfaces. The patterning by TPA then results in solid polymerized structures embedded in the non-exposed resin. The waveguide is then finally obtained by thermally treating the samples for 2 h at 200 °C in a nitrogen atmosphere. This particularly avoids any solvent-based processing (cf., Figure 4). Dependent on the chosen optoelectronic elements, data transfer rates as high a 7 Gbit/s at a bit error ratio of about 10^{-9} were routinely achieved.

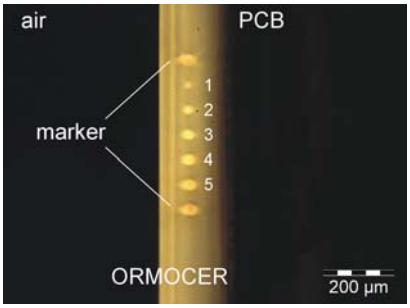

Fig. 15. TPA-WG fabricated by 2PP in a specially designed acrylate-based ORMOCER® after (Houbertz et al., 2008a). As laser source, a Ti:sapphire laser was used operating at 800 nm.

Another application example is related to the field of regenerative or biomedicine which attracts increasing attention. For example, micro-needle fabrication for drug delivery or the realization of scaffold structures using 2PP was already demonstrated (Doraiswamy et al., 2005; Narayan et al., 2005; Ostendorf & Chichkov, 2006). Scaffolds for medical applications provide 3D structures with well-defined shapes with an interconnecting pore structure in the range of a few up to several hundreds of µm, thus mimicking the properties of extracellular matrices. Such artificial matrices should support 3D cell formation, cell proliferation, and differentiation in order to create neo-tissue or grafts from autologous cell cultures.
The large-scale fabrication of biomedical scaffold structures with dimensions in the mm-range still remains very challenging from a technical and a materials' point of view. Most commercial rapid prototyping techniques cannot provide sufficiently small structure sizes

of a few μm in order to produce highly-porous scaffolds. Thus, 2PP with tailored material systems is a promising technology for this application, because it allows a real 3D fabrication at high resolution and a free design of the structures. In Figure 16, various highly-porous scaffolds fabricated by 2PP in OC-V/Ini2 are shown. An objective with a NA of 0.45 in the inverted configuration (cf., Figure 3 (c)) was used. It has to be mentioned, however, that the processing times are not yet optimized, and the equipment is continuously modified in order to reduce the necessary production time. This will be published elsewhere.

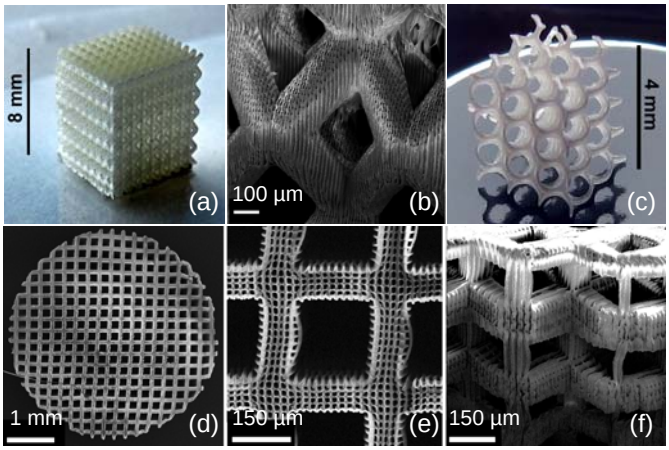

Fig. 16. Scaffolds fabricated by 2PP in OC-V/2 wt.-% Ini2. (a,b) Scaffold after a design from (Phoenix), redesigned by the authors, (c) scaffold after (Hart, 2009), and (d-f) scaffold with cubically designed pores of about 180 μm size (hatch distance 20 μm).

4. Conclusions

We have demonstrated the use of visible and infrared laser pulses for the fabrication of several types of sub-diffraction limit micro- and nanostructures by 2PP and 3PP. The data demonstrate that a well-defined fabrication of arbitrary structures can routinely be performed. The TPA cross-sections of some photoinitiators were characterized by the z-scan method, and were correlated to voxel size studies for differently functionalized hybrid polymers. First results on the fabrication of sub-100 nm features with a specially tailored hybrid material were presented as well. An investigation of the degree of organic cross-linking of patterns written by 2PP has yielded that it is comparable to the one achieved on conventionally UV-exposed ORMOCER® layers. First 3PP results demonstrate a significant circumvention of the diffraction limit, resulting in feature sizes of only $\lambda/7$ even without any optimization of process and material. Large-scale scaffolds up to the cm regime were fabricated using a modified TPA setup which has a huge potential for biomedical and tissue engineering applications. The scaffolds were fabricated with interconnecting pores, and a pore density as high as 90 % can be crated by using hybrid polymer materials due to their excellent mechanical stability. However, further work concerning the TPA cross-sections of initiators and voxel formation for differently functionalized materials including

investigations on the organic cross-linking by spectroscopic methods and mechanical stability investigations are presently carried out.

5. Acknowledgements

We thank Carola Cronauer and Adelheid Martin for their excellent support in materials synthesis, formulation, and characterization. Financial support from the Deutsche Forschungsgemeinschaft (grant: HO 2475/3-1), and from the Fraunhofer-Gesellschaft für Angewandte Forschung e.V. (Challenge Programme) is gratefully acknowledged. One of us (R.H.) would like to express special thanks to the friends who supported writing of this manuscript by providing continuous inspiration, particularly J.W. All colleagues who have contributed to our work by supporting us with discussions and other support are greatly appreciated.

6. References

Andrew, T. L.; Tsai, H. J. & Menon, R. (2009), Confining Light to Deep Subwavelength Dimensions to Enable Optical Nanopatterning, *Science* 324 (5929), 917-921

Asaka, S.; Nakanishi, S.; Itoh, H.; Kamada, M.; Watanabe, M.; Arimoto, O.; Fujiwara, S.; Tsujibayashi, T. & Itoh, M. (1998), Time-gated photon counting method for two-photon spectroscopy using synchrotron radiation and laser, *Review of Scientific Instruments* 69 (5), 1931-1933

BASF, initiators from Ciba-Geigy, now part of BASF

Baudach, S.; Bonse, J.; Krüger, J. & Kautek, W. (2000), Ultrashort pulse laser ablation of polycarbonate and polymethylmethacrylate, *Applied Surface Science* 154-155 (1-4), 555-560

Beyer, M.; Stichel, T.; Houbertz, R. & Sextl, G. (2010), Novel biocompatible hybrid polymers processed by two-photon polymerization (unpublished data)

Blanchet, G. B.; Fincher Jr., C. R.; Jackson, C. L.; Shah, S. I. & Gardner, K.H. (1993), Laser Ablation and the Production of Polymer Films, *Science* 29 (262). (5134), 719 – 721

Bowman, C. N. & Kloxin, C. J. (2008), Toward an Enhanced Understanding and Implementation of Photopolymerization Reactions, *AIChE Journal* 54 (11), 2775 – 2795

Bräuer, A.; Dannberg, P.; Mann, G. & Popall, M. (2001), Precise Polymer Micro-Optical Systems, *MRS Bulletin* 26, 519-522

Buestrich, R.; Kahlenberg, F.; Popall, M.; Dannberg, P.; Müller-Fiedler, R. & Rösch, O. (2001), ORMOCER®s for Optical Interconnection Technology, *Journal of Sol-Gel Science and Technology* 20, 181 – 186

Cheng, Y.; Sugioka, K.; Msuda, M.; Toyoda, K.; Kawachi, M.; Shihoyama, K. & Midorikawa, K. (2003), 3D microstructuring inside Foturan glass by femtosecond laser, *RIKEN Review*, No. 50, 101-106

Claeyssens, F.; Hasan, E. A.; Gaidukeviciute, A.; Achilleos, D. S.; Ranella, A.; Reinhardt, C.; Ovsianikov, A.; Xiao, S.; Fotakis, C.; Vamvakaki, M.; Chichkov, B. N. & Farsari, M. (2009), Three-dimensional biodegradable structures fabricated by two-photon polymerization, *Langmuir* 25 (5), 3219–3223

Conforti, P. F.; Prasad, M. & Garrison, B.J. (2007), Simulations of Laser Ablation of Poly(methyl methacrylate): Fluence versus Number of Photons, *Journal of Physical Chemistry C* 111 (32), 12024–12030

Cumpston, B. H.; Ananthavel, S. P.; Barlow, S.; Dyer, D. L.; Ehrlich, J. E.; Erskine, L. L.; Heikal, A. A.; Kuebler, S. M.; Lee, I. Y. S.; McCord-Maughon, D.; Qin, J.; Rockel, R.; Rumi, M.; Wu, X.-L.; Marder, S. R. & Perry, J. W. (1999), Two-photon polymerization initiators for three-dimensional optical data storage and microfabrication, *Nature* 398, 51–54

Declerck, P. (2010), Synthesis and technological processing of hybrid inorganic-organic materials for photonic applications, *Dissertation*, Julius-Maximilian University Würzburg

Denk, W.; Strickler, H. & Webb, W. (1990), 2-Photon Laser Scanning Fluorescence Microscopy, *Science* 6, 248 (4951), 73-76

Denk, W. & Svoboda, K. (1997), Photon upmanship: why multiphoton imaging is more than a gimmick, *Neuron* 18 (3), 351–357

Deubel, M.; v. Freymann, G.; Wegener, M.; Pereira, S.; Busch, K. & Soukoulis, C. M. (2004), Direct laser writing of three-dimensional photonic-crystal templates for telecommunications, *Nature Materials* 3, 444-447

Doraiswamy, A.; Platz, T.; Narayan, R. J.; Chichkov, B.; Ovsianikov, A.; Houbertz, R.; Modi, R.; Auyeung, R. & Chrisey, D. B. (2005), Biocompatibility of CAD/CAM ORMOCER® polymer scaffold structures, *Materials Research Society Symposium Proceedings* 845, AA2.4.1

El-Batahgy, A. M. (1997), Effect of laser welding parameters on fusion zone shape and solidification structure of austenitic stainless steels, *Materials Letters* 32 (2-3), 55-163

Fodermeyer, V. (2009), Spektroskopische Untersuchung zur lichtinduzierten Vernetzung von Hybridpolymeren, *Diploma Thesis*, Julius-Maximilian University, Würzburg

Fuchs, U.; Zeitner, U. D. & Tünnermann, A. (2006), Hybrid optics for focusing ultrashort laser pulses, *Optics Letters* 31 (10), 1516-1518

Gittard, S. D.; Ovsianikov, A.; Akar, H.; Chichkov, B.; Monteiro-Riviere, N. A.; Stafslien, S.; Chisholm, B.; Shin, C. C.; Shih, C. M.; Lin, S. J.; Su, Y. Y. & Narayan, R. J. (2010), Two Photon Polymerization-Micromolding of Polyethylene Glycol-Gentamicin Sulfate Microneedles, *Advanced Engineering Materials* 12 (4), B77-B82

Göppert-Mayer, M. (1931), Über Elementarakte mit zwei Quantensprüngen, *Annalen der Physik* 401 (3), 273–294

Haas, K.-H. & Wolter, H. (1999), Synthesis, properties and applications of inorganic-organic copolymers (ORMOCER®s), *Current Opinion in Solid State and Materials Science* 4, 571–580

Haas, K.-H. (2000), Hybrid Inorganic-Organic Polymers Based on Organically Modified Si-Alkoxides, *Advanced Engineered Materials* 2, 571 – 582

Haas, K.-H. & Wolter, H. (2001), Properties of Polymer-Inorganic Composites, *Encyclopedia of Materials: Science and Technology* Oxford, Elsevier: 7584-7594

Haas, U.; Haase, A.; Satzinger, V.; Pichler, H.; Leising, G.; Jakopic, G.; Stadlober, B.; Houbertz, R.; Domann, G. & Schmitt, A. (2006), Hybrid polymers as tunable and directly-patternable gate dielectrics in organic thin-film transistors, *Physical Review B* 73, 235339.1-235339.7

Hart, G.W (2009), http : //www.georgehart.com/rp/rp.html

Haske, W.; Chen, V. W.; Hales, J. M.; Dong, W. T.; Barlow, S.; Marder, S. R. & Perry, J. W. (2007), 65 nm feature sizes using visible wavelength 3-D multiphoton lithography, *Optics Express* 15 (6), 3426-3436

Helmerich, A.; Raether, F.; Peter, D. & Bertagnolli, H. (1994), Structural studies on an ORMOCER® system containing zirconium, *Journal of Materials Science* 29, 1388 – 1393

Houbertz, R.; Froehlich, L.; Schulz, J. & Popall, M. (2001), Inorganic-Organic Hybrid Materials (ORMOCER®s) for Multilayer Technology - Passivation and Dielectric Behavior, *Materials Research Society Symposium Proceedings* 665, 321 – 326

Houbertz, R.; Schulz, J.; Froehlich, L.; Domann, G. & Popall, M. (2003a), Inorganic-organic hybrid materials for polymer electronic applications, *Materials Research Society Symposium Proceedings* 769, 239-244

Houbertz, R.; Domann, G.; Cronauer, C.; Schmitt, A.; Martin, H.; Park, J.-U.; Fröhlich, L.; Buestrich, R.; Popall, M.; Streppel, U.; Dannberg, P.; Wächter, C. & Bräuer, A. (2003b), Inorganic-organic hybrid materials for application in optical devices, *Thin Solid Films* 442, 194–200

Houbertz, R.; Domann, G.; Schulz, J.; Olsowski, B.; Fröhlich, L. & Kim, W. S. (2004), Impact of photoinitiators on the photopolymerization and the optical properties of inorganic-organic hybrid polymers, *Applied Physics Letters* 84 (7), 1105–1107

Houbertz, R.; Wolter, H.; Dannberg, P.; Serbin, J. & Uhlig, S. (2006), Advanced packaging materials for optical applications: bridging the gap between nm-size structures and large-area panel processing, *Proceedings of SPIE* 6126, 612605.1-612605.13, doi: 10.1117/12.660140

Houbertz, R. (2007), http://www.fraunhofer.de/ueber-fraunhofer/wissenschaftliche-exzellenz/fraunhofer-wissenschaftspreise/archiv/

Houbertz, R.; Satzinger, V.; Schmid, V.; Leeb, W. & Langer, G. (2008a), Optoelectronic printed circuit board: 3D structures written by two-photon absorption, *Proceedings SPIE* 7053, 70530B.1 -70530B.13

Houbertz, R.; Declerck, P.; Passinger, S.; Ovsianikov, A.; Serbin, J. & Chichkov, B. N. (2008b), Investigations on the generation of photonic crystals using two-photon polymerization (2PP) of inorganic-organic hybrid polymers with ultra-short laser pulses, In: *Nanophotonic Materials: Photonic Crystals, Plasmonics, and Metamaterials*, R.W. Wehrspohn, H.S. Kitzerow, & K. Busch (Eds.) , 97-114, Wiley VCH, 978-3-527-40858-0, Weinheim, 97 - 113

Houbertz, R.; Steenhusen, S.; Beyer, M. & Sextl, G. (2010) (unpublished data)

Jia, B. H.; Serbin, J.; Kim, H.; Lee, B.; Li, J. F. & Gu, M. (2007), Use of two-photon polymerization for continuous gray-level encoding of diffractive optical elements, *Applied Physics Letters* 90, 073503.1-073503.3

Kawata, S.; Sun, H. B.; Tanaka, T. & Takada, K. (2001), Finer features for functional microdevices, *Nature* 412 (6848), 697–698

Koechlin, M.; Poberaj, G. & Günter, P. (2009), High-resolution laser lithography system based on two-dimensional acousto-optic deflection, *Review of Scientific Instruments* 80, 085105

Landgraf, F. (2010), Spektroskopische Untersuchung zur UV-induzierten Vernetzung von Hybridpolymeren, Diploma Thesis, FH Regensburg

Li, J.; Jia, B. & Gu, M. (2008), Engineering stop gaps of inorganic-organic polymeric 3D woodpile photonic crystals with post-thermal treatment, *Optics Express* 16 (24), 20073-20080

Li, L. J.; Gattass, R. R.; Gershgoren, E.; Hwang, H. & Fourkas, J. T. (2009), Achieving lambda/20 Resolution by One-Color Initiation and Deactivation of Polymerization, *Science* 324 (5929), 910-913

Maruo, S.; Nakamura, O. & Kawata, S. (1997), Three-dimensional microfabrication with two-photon-absorbed photopolymerization, *Optics Letters* 22 (2), 132-134

Narayan, R. J.; Jin, C.; Doraiswamy, A.; Mihailescu, I. N.; Jelinek, M.; Ovsianikov, A.; Chichkov, B. N. & Chrisey, D. B. (2005), Laser Processing of Advanced Bioceramics, *Advanced Engineered Materials* 7 (12), 1083-1098

Nolte, S.; Will, M.; Burghoff, J. & Tünnermann, A. (2004), Ultrafast laser processing: new options for three-dimensional photonic structures, *Journal of Modern Optics* 51 (16-18), 2533-2542

Odian, G. (1981), *Principles of polymerization*, Wiley-Interscience, New York, 2nd edition

Ostendorf, A. & Chichkov, B.N. (2006), Two-Photon Polymerization: A new Approach to Micromachining, *Photonics Spectra*, October Issue

Phoenix GmbH & Co. KG, Gröbenzell, Germany

Robertsson, M. E.; Hagel, O. J.; Gustafsson, G.; Dabek, A.; Popall, M.; Cergel, L.; Wennekers, P.; Kiely, P.; Lebby, M. & Lindhal, T. (1998), O/e-MCM Packaging with New, Patternable Dielectric and Optical Materials, *Proceedings 48th Electronic Component Technology Conference* (Seattle, Washington, USA), IEEE Catalogue No. 98CH36206, 1413-1421

Rousseau, A. & Boutevin, B. (1992), Synthesis of low absorption halogenated polymers for POF, *Proceedings of the Plastic Optical Fibers Conference*, 33–37, Paris, June 22-23, 1992

Sanchez, C.; Julián, B. ; Belleville, Ph. & Popall, M. (2005), Applications of hybrid organic–inorganic nanocomposites, *Journal Materials Chemistry* 15, 3559–3592

Schafer, K. J.; Hales, J. M.; Balu, M.; Belfield, K. D.; Van Stryland, E. W. & Hagan, D. J. (2004), Two photon absorbtion cross-sections of common photoinitiators, *Journal Photochemistry and Photobiology* A162, 497–502

Schizas, C.; Melissinaki, V.; Gaidukeviciute, A.; Reinhardt, C.; Ohrt, C.; Dedoussis, V.; Chichkov, B. N.; Fotakis, C.; Farsari, M. & Karalekas, D. (2010), On the design and fabrication by two-photon polymerization of a readily assembled micro-valve, *International Journal of Advanced Manufacturing Technology* 48 (5-8), 435-441

Schweizer, Th.; Neumeister, A.; Guo, Q.; Wohlleben, W.; Leyrer, R. J.; Kling, R. & Ostendorf, A. (2008), Generation of Photonic Crystal End Faces Using Laser Microfabrication, *JLMN - Journal of Laser Micro/Nanoengineering* 3 (3), 141-146

Seidl, B. & R. Liska (2007), Mechanistic investigations on a diynone type photoinitiator, *Macromolecular Chemistry and Physics* 208 (1), 44-54

Serbin, J.; Egbert, A.; Ostendorf, A.; Chichkov, B. N.; Houbertz, R.; Domann, G.; Schulz, J.; Cronauer, C.; Fröhlich, L. & Popall, M. (2003), Femtosecond laser-induced two-photon polymerization of inorganic–organic hybrid materials for applications in photonics, *Optics Letters* 28, 301-303

Serbin, J.; Ovsianikov, A. & Chichkov, B. N. (2004), Fabrication of woodpile structures by two-photon polymerization and investigation of their optical properties, *Optics Express* 12 (21), 5221–5228

Sheikbahae, M.; Said, A. A. & Vanstryland, E. W. (1989), High-sensitivity, single-beam n_2 measurements, *Optics Letters* 14 (17), 955–957

Sheikbahae, M.; Said, A. A.; Wei, T. H.; Hagan, D. J. & Vanstryland, E. W. (1990), Sensitive measurement of optical nonlinearities using a single beam, *IEEE Journal of Quantum Electronics* 26 (4), 760–769

Sieben, M. & Brunnecker, F. (2009), Welding plastic with lasers, *Nature Photonics* 3, 270–272

Simchi, A. (2006), Direct laser sintering of metal powders: Mechanism, kinetics and microstructural features, *Materials Science and Engineering A* 428, 148–158

Song, J. H.; O'Brien, P. & Peters, F. H. (2009), Optimal laser welding assembly sequences for butterfly laser module packages, *Optics Express* 17 (19), 16406-16414

Spyridaki, M.; Koudoumas, E.; Tzanetakis, P.; Fotakis, C.; Stoian, R.; Rosenfeld, A. & Hertel, I. V. (2003), Temporal pulse manipulation and ion generation in ultrafast laser ablation of silicon, *Applied Physics Letters* 83 (7), 1474–1476

Stampfl, J.; Fouad, H.; Seidler, S.; Liska, R.; Schwager, F.; Woesz, A. & Fratzl, P. (2004), Fabrication and moulding of cellular materials by rapid prototyping, *Int. J. Materials and Product Technology* 21 (4), 285-296

Steenhusen, S. (2008), Mikrostrukturierung von Hybridpolymeren mit Zwei-Photonen-Absorption, *Diploma Thesis*, Julius-Maximilian University Würzburg.

Steenhusen, S.; Stichel, T.; Houbertz, R. & Sextl, G. (2010a), Multi-photon polymerization of inorganic-organic hybrid polymers using visible or IR ultrafast laser pulses for optical or optoelectronic devices, *Proceedings of SPIE* 7591, 759114.1–759114.12

Steenhusen, S.; Houbertz, R. & Sextl, G. (2010b), 3D sub-diffraction limit patterning of hybrid polymers with visible and infrared laser pulses, *Proceedings Laser Precision Micromachining LPM 2010*, Stuttgart, June 7-10, 2010

Stichel, T.; Houbertz, R.; Hecht, B. & Sextl, G. (2010), Two-photon polymerization as method for the fabrication of large scale biomedical scaffold applications, *Proceedings Laser Precision Micromachining* LPM 2010, Stuttgart, June 7-10, 2010

Streppel, U.; Dannberg, P.; Wächter, Ch.; Bräuer, A.; Fröhlich, L.; Houbertz, R. & Popall, M. (2002), New wafer-scale fabrication method for stacked optical waveguide interconnects and 3D micro-optic structures using photoresponsive (inorganic-organic hybrid) polymers, *Optical Materials* 21, 475 –483

Studer, K.; Decker, Ch.; Beck, E. & Schwalm, R. (2003), Overcoming oxygen inhibition in UV-curing of acrylate coatings by carbon dioxide inerting, Part I, *Progress in Organic Coatings* 48, 92–100

Sun, H. B.; T. Tanaka & Kawata, S. (2002), Three-dimensional focal spots related to two-photon excitation, *Applied Physics Letters* 80 (20), 3673-3675

Tanaka, T.; Sun, H. B. & Kawata, S. (2002), Rapid sub-diffraction-limit laser micro/ nanopro-cessing in a threshold material system, *Applied Physics Letter* 80 (2), 312-314

Uhlig, S.; Fröhlich, L.; Chen, M.; Arndt-Staufenbiel, N.; Lang, G.; Schröder, H.; Houbertz, R.; Popall, M. & Robertsson, M. (2006), Polymer optical interconnects - a scalable large-area panel processing approach, *IEEE Transactions Advanced Packaging* 29, 158–170

Wojcik, A. B. & Klein, L. C. (1995), Transparent Inorganic/Organic Copolymers by the Sol-Gel Process: Copolymers of Tetraethyl Orthosilicate (TEOS), Vinyl Triethoxysilane (VTES) and (Meth)arcylate Monomers, *Journal of Sol-Gel Science and Technology* 4, 57–66

Van Stryland, E. W. & Sheikbahae, M. (1998), Z-scan measurements of optical nonlinearities, In: *Characterization Techniques and Tabulations for Organic Nonlinear Materials*, Kuzyk, M. and Dirk, C. (eds.), 655–692, Marcel Dekker Inc., 978-0824799687 New York

Wei, F. (2010), http : //www.eng.nus.edu.sg/LCEL/RP/u21/wwwroot/stl library.htm

Wong, S.; Deubel, M.; Pérez-Willard, P.; John, S.; Ozin, G. A.; Wegener, M. & von Freymann, G. (2006), Direct Laser Writing of Three-Dimensional Photonic Crystals with a Complete Photonic Bandgap in Chalcogenide Glasses, *Advanced Materials* 18 (3), 265-269

Yamaguchi, S. & Tahara, T. (2003), Two-photon absorption spectrum of all-trans retinal, *Chemical Physics Letters* 276 (1-2), 237-243